ACS NANO
Cite This: ACS Nano 2018, 12, 8588–8596
www.acsnano.org

ARTICLE

Bionic Single-Electrode Electronic Skin Unit Based on Piezoelectric Nanogenerator

Xiaoxiong Wang,[†,⊥] Wei-Zhi Song,[†,⊥] Ming-Hao You,[†] Jun Zhang,[†] Miao Yu,[†,‡] Zhiyong Fan,[§] Seeram Ramakrishna,[∥] and Yun-Ze Long*[,†]

[†]Collaborative Innovation Center for Nanomaterials & Devices, College of Physics, Qingdao University, Qingdao 266071, China
[‡]Department of Mechanical Engineering, Columbia University, New York, New York 10027, United States
[§]Department of Electronic & Computer Engineering, The Hong Kong University of Science & Technology, Kowloon, Hong Kong, China
[∥]Center for Nanofibers & Nanotechnology, National University of Singapore, Singapore 119077, Singapore

Supporting Information

ABSTRACT: **Moravec's paradox shows that low-level sensorimotor skills are more difficult than high-level reasoning in artificial intelligence and robotics. So simplifying every sensing unit on electronic skin is critical for endowing intelligent robots with tactile and temperature sense. The human nervous system is characterized by efficient single-electrode signal transmission, ensuring the efficiency and reliability of information transmission under big data conditions. In this work, we report a sensor based on a single-electrode piezoelectric nanogenerator (SPENG) by electrospun polyvinylidene fluoride (PVDF) nanofibers that can realize steady-state sensing of pressure integrating cold/heat sensing on a single unit. Piezoelectric signals appear as square wave signals, and the thermal-sensing signals appear as pulse signals. Therefore, the two signals can be acquired by a single unit simultaneously. The SPENG overcomes the shortcoming of electronic skins based on a single-electrode triboelectric nanogenerator (STENG), which can sense only dynamic movement and cannot sense temperature variations. The new sensor configuration uses a capacitor instead of the STENG's ground wire as a potential reference, allowing it to be used for truly autonomous robots. At the same time, the traditional advantages of polymer piezoelectric materials, such as flexibility, transparency, and self-powered advantages, have also been preserved.**

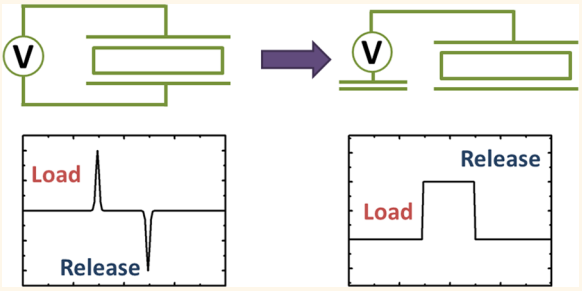

KEYWORDS: *single-electrode sensor, piezoelectric nanogenerators, polyvinylidene fluoride, electrospinning, electronic skin*

Moravec's paradox shows that low-level sensorimotor skills such as vision or tactile sense are more complex than high-level reasoning skills in the artificial intelligence and robotics area.[1] The vision problem has been solved by current artificial intelligence,[2] but the tactile sense will rely more on senor performance in this early stage, which should be simplified as much as possible to reduce information processing complexity. Typically, there are five types of flexible sensing electronic units that can perform as input devices for electronic skin (e-skin), including piezoresistive,[3,4] piezoelectrical,[5−7] capacitive,[8] field effect transistor,[9,10] and triboelectric nanogenerator (TENG)[11−13] based devices, which can perform as input units on bionic skin. Recently, a triboelectric sensor based on a single-electrode TENG (STENG) has reduced the two electrodes to one,[14,15] reducing the complexity of the electronic skin, which possesses thousands of units in a small area. However, TENG-based electronic skin is more applicable for dynamic tracing, and it cannot give information about temperature. Actually, the single-electrode sensor relies on charge transfer, which can be achieved by most nanogenerators. So a sensor based on a piezoelectric nanogenerator (PENG) will also realize a single-electrode configuration.

As an excellent polymer piezoelectric material, polyvinylidene fluoride (PVDF) has flexibility, low density, low thermal conductivity, and high chemical stability, which is in coherence with human skin.[16,17] With its piezoelectricity, PVDF can be used for tactile sensor arrays, inexpensive strain gauges, and lightweight audio transducers.[18,19] Electrospun PVDF ultrathin fibers can be used directly for power generation and sensing without routine polarization.[20] High pressure, solvent volatilization, and stretching of PVDF during the electrospinning process lead to the formation of a β-phase, which favors the

Received: June 4, 2018
Accepted: August 13, 2018
Published: August 13, 2018

DOI: 10.1021/acsnano.8b04244
ACS Nano 2018, 12, 8588–8596

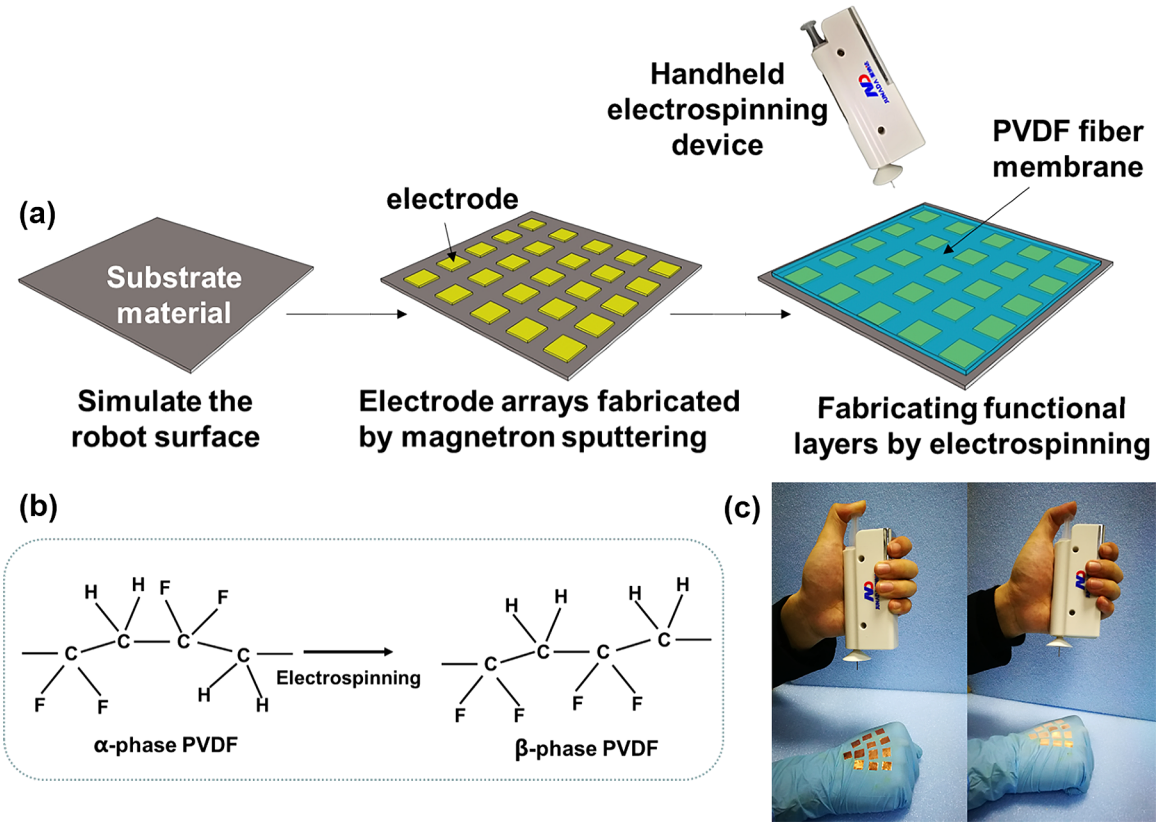

Figure 1. Fabricating single-electrode e-skin. (a) Fabrication process flow. (b) Changes in PVDF molecular structure during electrospinning. (c) Photograph of the process of fabricating the e-skin by using a hand-held electrospinning device.

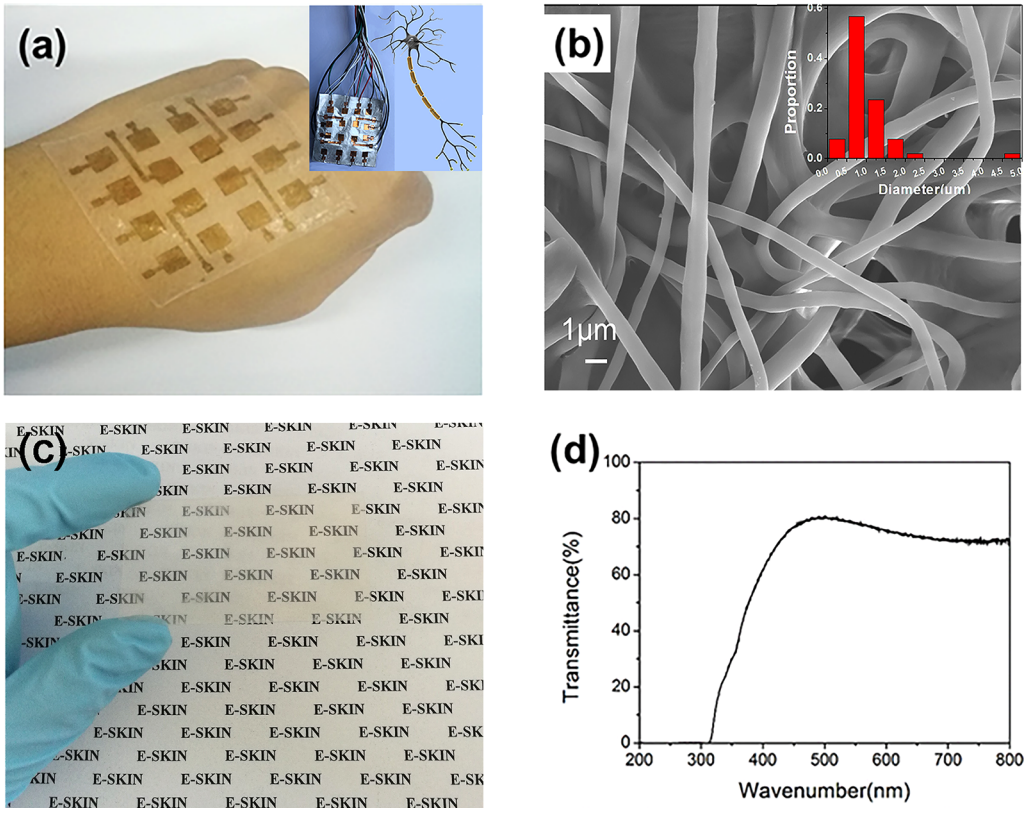

Figure 2. Structure and some properties of the e-skin in two different forms. (a) Photograph of the e-skin on a gold electrode. Inset shows the demonstration of its analog to a neuron cell. (b) Representative SEM images and nanofiber distribution graphs of the PVDF film. (c) Transparency form of the e-skin using ITO electrodes. (d) UV−vis absorption spectra of the e-skin with ITO electrodes.

DOI: 10.1021/acsnano.8b04244
ACS Nano 2018, 12, 8588−8596

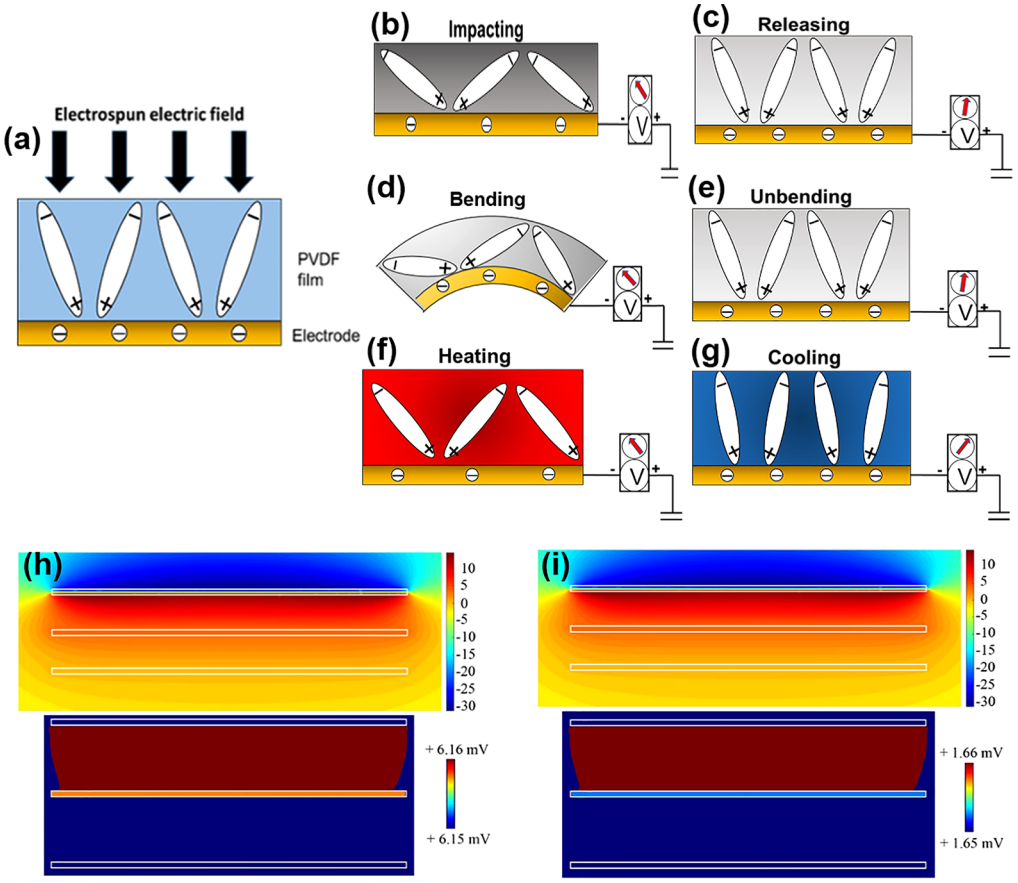

Figure 3. Working mechanism of the single-electrode e-skin. (a) Structure and principle of the e-skin. (b, c) Electric signal due to the piezoelectric effect from the device when impact and release strain is applied. (d, e) Electric signal due to the piezoelectric effect from the device when bending and unbending is applied. (f, g) Electric signal due to the pyroelectric effect from the device when heating and cooling is applied. (h, i) Calculated electric potential distribution before and after change of the electric dipole. From top to bottom are the piezoelectric layer, the primary electrode, and the reference electrode. The lower scale bar below shows the variation of electric potential from 3.6 V.

generation of piezoelectric and pyroelectric effects.[21,22] In addition, the high-voltage electrostatics of the spinning process make the electrical dipole moment in the deposited PVDF lean toward the vertical film plane.[23] Electrospinning facilitates the preparation of large-scale fiber membranes, leading to the scale production of such an electronic skin.

In this work, we report a single-electrode piezoelectric nanogenerator (SPENG) based on electrospun PVDF nanofibers that can realize steady-state sensing of pressure-integrating cold/heat sensing on a single unit. The single-electrode configuration introduces steady-state sensing, so that when the pressure is maintained, there will be a voltage output, and when the pressure is removed, the voltage disappears; this piezoelectric voltage depends only on the pressure and does not change as the sensor area changes. Moreover, cold and hot sensing shows a pulse signal, so it can be easily separated from the pressure signal. Transparent sensor performance can be achieved with indium tin oxide (ITO) glass and can be easily applied to transparent interfaces. We tested the electronic skin pressure, temperature-sensing performance, and mapping. Due to the use of cost-efficient PVDF and electrospinning, the preparation method is extremely simple. Therefore, this method can be manufactured on a large scale and at a low cost. The SPENG may be used in future functional systems such as robots.

RESULTS AND DISCUSSION

Basic Characterization of the E-Skin. The photographs, scanning electron microscopy (SEM) images, transparency, and UV−vis absorption spectra of the self-powered e-skin based on PVDF nanofibers are shown in Figure 2. The e-skin is synthesized by a high-voltage electrospinning method, as shown in Figure 2a. It can be seen from the figure that the e-skin has good flexibility and good fit with the skin. As can be seen from Figure 2b, the electrospun PVDF nanofibers have an average diameter of 993 nm with a diameter distribution (standard deviation) of 631 nm, obtained by measuring 51 sites' fiber diameters evenly distributed in SEM photographs.

Figure 2c is a photograph of the e-skin with ITO electrodes, showing its good transparency. As shown in the UV−vis spectra (Figure 2d), the transmittance of the e-skin with ITO electrodes at 500−800 nm is about 70%. The visible transmittance of ITO is about 90%. The absorption edge at about 400 nm can be attributed to the free radicals and ions in PVDF.[25] Polymers may contain free radicals, carbanions, and carbonium ions. In these segments the carbon atoms are supposed to carry unhybridized p-orbitals, which can form molecular orbitals with the p-orbitals of unsaturated systems. The molecular orbitals and the energy levels of these three systems should be very similar, and they exhibit absorption bands in the same region.[26]

DOI: 10.1021/acsnano.8b04244
ACS Nano 2018, 12, 8588−8596

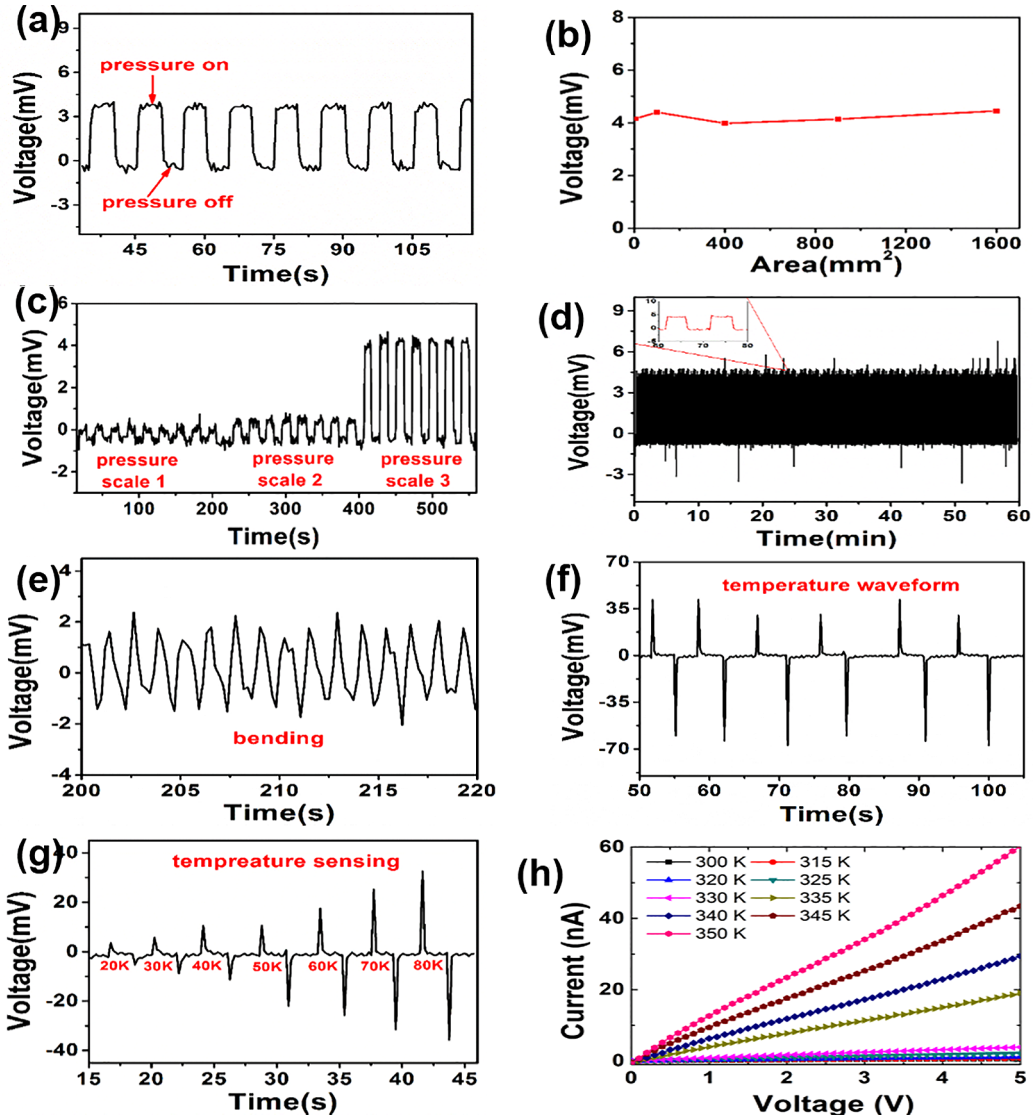

Figure 4. Open-circuit voltage signal of the e-skin under different conditions: (a) under 0.1 Hz repeated compressive impacts, (b) under the same pressure, but different membrane area, (c) with the same membrane area, but different pressures, (d) under repeated compressive impacts for 60 min, and (e) under 0.8 Hz repeated bending and unbending. (f) The same temperature contrast is applied under the same temperature. (g) The same temperature gradient is applied at different initial temperature. (h) *I*–*V* curve of PVDF under different temperatures.

Working Mechanism of the Single-Electrode E-Skin. Figure 3 shows the working mechanism of a single-electrode e-skin based on piezoelectric and pyroelectric effects. We creatively changed the ground wire in the previous single-electrode structure[27] to a large capacitor, which can free robots and other equipment from the control of the ground wire, which lets them move around freely. PVDF was spontaneously polarized in the electrospinning process, and the electric dipole arrangement of the film is shown in Figure 3a. The d_{33} of the PVDF film is about 6 pC/N. The electric dipoles remain in an equilibrium state because the spontaneous polarization of PVDF is constant at room temperature.[28] When the impact force is applied on the PVDF film, the film is compressed and the total spontaneous polarization decreases significantly; then the open-circuit voltage between the electrode and one pole of the capacitor will change (Figure 3b). On the other hand, the voltage change will disappear and return to its original state due to the polarization recovering when the impact force is released (Figure 3c). Under open-circuit conditions, where the load impedance is infinite, the piezoelectric open voltage (V_{piezo}) can be expressed by the equation[29]

$$V_{piezo} = A \times \frac{d_{33}}{\varepsilon_{33}^{T}} \times h \times \Delta\sigma \quad (1)$$

where A is a constant, d_{33} is the piezoelectric coefficient ($C \cdot N^{-1}$), ε_{33}^{T} is the permittivity at constant stress in the polarization direction, h is the thickness, and $\Delta\sigma$ is mechanical stress. At the same time, if we apply a compressive strain in the transverse direction of the e-skin, it will bend, a negative potential is created on the compression side of the film, then a negative pulse is observed, and a positive potential is generated when it is released as shown in Figure 3d,e.[28]

When warming PVDF, electric dipoles oscillate within a larger degree of their respective aligning axes range, which significantly decreases the strength of the spontaneous polarization;[30,31] then PVDF shows a positive open-circuit voltage output signal (Figure 3f). On the other hand, when

DOI: 10.1021/acsnano.8b04244
ACS Nano 2018, 12, 8588–8596

cooling the PVDF, the electric dipole oscillation amplitude is significantly reduced, which increases the polarization. Then the PVDF shows a negative open-circuit voltage output signal (Figure 3g). Under open-circuit conditions, where the load impedance is infinite, the pyroelectric open voltage (V_{pyro}) can be expressed by the equation[29]

$$V_{pyro} = A \times \frac{p}{\varepsilon_{33}^{T}} \times h \times \Delta T \quad (2)$$

where p is a pyroelectric coefficient and ΔT is the change in temperature.

The electric dipoles absorb the electric charge in the natural environment, especially in a high-humidity environment, and are shielded. However, when PVDF is pressed, the electric dipole moment drops, resulting in a surplus of electrons at the bottom electrode, thereby forming a lower potential with respect to the reference electrode. According to the voltage meter connected to the configuration shown in Figure 3b, which represents an open circuit, we can obtain a positive voltage. When the pressure is removed, the electric dipole moment recovers, causing the excess charge to be regained, recovering shielding and a zero potential difference will be obtained, as shown in Figure 3c. Bending also leads to a decrease in the electric dipole moment, resulting in a similar effect, as shown in Figure 3d,e. The change of the electric dipole moment caused by heating and cooling is opposite, and therefore opposite potential differences are generated, as shown in Figure 3f,g. Using the above model, the electric potential distribution before and after the application of pressure was calculated utilizing COMSOL software (Figure 3h,i). From top to bottom are the piezoelectric layer, the primary electrode, and the reference electrode. The electric displacement field before and after applying pressure are 8 and 7.99 μC m^{-2}.[32] It can be seen from the figure that the electric dipole moment without adsorbing charge can form a high electric field at the primary electrode, and the value given in the calculation is about 3.6 V. The electric field attenuates much faster with increasing the distance than the field generated by the monopole space charge.[32] The typical electric potential generated by such electric displacement is in volts instead of the kilovolts generated by monopole space charge, as reported by STENGs. However, a smaller electric field makes the dielectric less affected by leakage.[32] After the charge is absorbed, the system enters a steady state. After the pressure is applied, the spatial electric field will change slightly, which needs amplification to be seen. Therefore, in Figure 3h,i, we placed a potential map with a reference potential of 3.6 V. It can be seen that the relative potential at the primary electrode before pressing is about 6.15 mV, and the relative potential at the primary electrode is reduced to about 1.65 mV after pressing, resulting in a potential change of 4.5 mV. This change in potential difference causes the main electrode to desorb some negative charge, causing the voltmeter to measure a potential difference of +4.5 mV.

Pressure- and Warmth-Sensing Performance of the E-Skin. Figure 4 shows the open-circuit voltage signal of the e-skin under different conditions and test instruments. From the different voltage waveforms it is easy to distinguish between different external influences on the e-skin. Figure 4a shows the open-circuit voltage output signal of the e-skin under 0.1 Hz repeated compressive impacts (device diagram shown in Figure S3a). In this process, the impact and release for each cycle lasts 5 s, respectively. When the impact force continues to be applied to the electronic skin, the electronic skin will have a stable open-circuit voltage output. When this force disappears, the voltage returns to its original state. Just like human skin, when touched by something the e-skin will sense that, and when the force disappears it cannot sense it. Figure 4b shows the open-circuit voltage of the e-skin of different working areas (the area of the impact stage is larger than the area of the film) under the same intensity of pressure. It is easy to see that the strength of the output signal has nothing to do with the membrane area. Therefore, the array unit of our e-skin can be made very small to increase the resolution of the e-skin. From the results of our current tests, this unit can be as small as 4 mm^2, which can be further minimized with more sophisticated wire access. Figure 4c shows the open-circuit voltage for one array unit of the e-skin under different pressures. As the pressure increases, the output voltage also increases. The pressures shown are approximately 3, 9, and 53 N, and the relevant setup is shown in Figure S12. From the signal-to-noise ratio, this e-skin can measure the pressure down to about 1 N. For smaller pressure, the noise signal is large and smoothing may be needed before the signal can be analyzed. As given by eq 1, the voltage is proportional to the mechanical stress. Just like human skin, the more powerful of the force, the more "pain" it will "feel". Then we tested the stability and durability of the e-skin, as shown in Figure 4d. Under repeated compressive impacts for 60 min, the output of the e-skin remains stable. It shows that our e-skin has excellent durability and stability. Last, we tested the voltage output of the e-skin under 0.8 Hz repeated bending and unbending (device diagram shown in Figure S3b), as shown in Figure 4e. As shown in the working mechanism of Figure 3d,e, a negative potential is created on the compression side of the film, and a negative pulse is observed; then a positive potential is generated when it is released, and a positive pulse is observed.

In order to observe the corresponding voltage of the e-skin at different temperatures, we used the heating film to provide a variety of temperature gradients for the e-skin. The open-circuit voltage due to the pyroelectric effect can be derived as[33]

$$V = \frac{A\Delta\sigma}{C} = \frac{A}{A'} \times \frac{\Delta\sigma d}{\varepsilon_r\varepsilon_0} = \frac{A}{A'} \times \frac{d}{\varepsilon_r\varepsilon_0}\Delta T \quad (3)$$

Here, d, A', and C are thickness, total area, and capacitance of the PVDF in the e-skin, respectively. Since the area of the heating film is larger than the area of the e-skin, the effective area is equal to the total area, so the open-circuit voltage is related only to the temperature difference. The heating film (Figure S3c) is set at a higher temperature. When the e-skin contacts the heating film it will have a positive voltage spike output, and when the e-skin leaves the heating film, there is a negative voltage spike output (Figure 4f). It is different from the square wave pulse of Figure 4a. So we can distinguish the pressure and temperature according to the waveform of the output voltage simulating the function of the e-skin. Figure 4g shows the open-circuit voltage of the e-skin when it touches and leaves the heating film at different temperatures (room temperature, 17 °C). As the heating film warms, the temperature difference gradually increases, and the voltage output also increases. Just like human skin, when contacting objects having different temperatures, it will "feel" different. The temperature-sensing performance maintains a pulse waveform, which can be attributed to the leakage effect. As known, the resistivity of the insulator drops with increasing

DOI: 10.1021/acsnano.8b04244
ACS Nano 2018, 12, 8588−8596

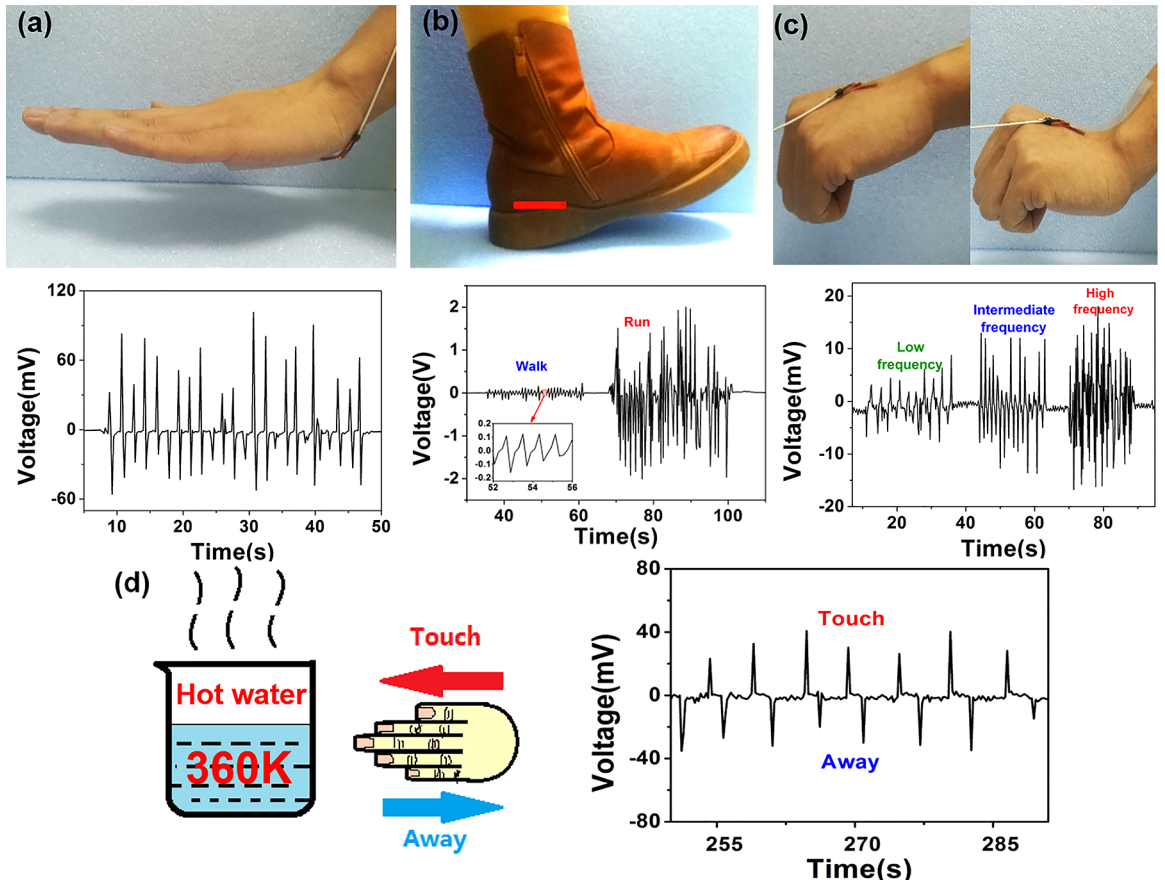

Figure 5. (a, b, c) Photographs of the e-skin on a hand, heel, and joint imitating patting a table, walking, running, and different frequency bending and the corresponding output voltage. (d) Simulated a hand touching and moving away from a hot water cup (~87 °C) with e-skin and the corresponding output voltage.

temperature. This is due to the thermal energy activating electrons from the valence band to the conduction band, generating conduction electrons and holes. It is still a challenge to determine the resistivity of PVDF, which is solved by using a configuration with an area of about 1 cm^2 and thickness of about 1 μm. From Figure 4h, it can be seen that as the temperature increases, the resistance of the PVDF decreases significantly, showing an increment of leakage current under the same electric field, which consumes the little charge generated by pyroelectricity, causing a pulse-like waveform.

E-Skin Sensing Mechanical Movement and the Prosthesis Touch Simulation. Based on the e-skin's superior performance, we further demonstrated the application of the e-skin in sensing a body's mechanical movement and in a simulation of a prosthesis touching hot things, as shown in Figure 5. Figure 5a shows the real-time pulse signals recorded by the e-skin on the palm when the hand slaps a table. According to the obtained results, the maximum positive and negative peak voltage are about 60 and −40 mV. A positive voltage is output when the hand hits, and a negative voltage is output when the hand raises; it is easy to see that the output is uneven because of the power to pat the table is not stable. Figure 5b shows the voltage output of the e-skin on the heel when walking and running. The output is similar to that by patting the table. The maximum positive and negative peak voltage outputs from the e-skin during walking and running are 0.1, −0.1, 1.25, and −1.5 V, respectively. In order to obtain the output voltage of the e-skin when the joint is bent, the e-skin is fixed on the wrist. As shown in Figure 5c, the output voltages at different bending frequencies are different. At low frequency (about 0.4 Hz), the output voltage ranged from −7 to 5 mV. When the frequency increased to intermediate, the voltage output ranged from −8 to 10 mV. Last, when the frequency increased to 1.6 Hz (high frequency), the output ranged from −16 to 14 mV. So our e-skin can easily sense mechanical movement such as patting a table, walking, running, or joint bending, which corresponds to sensing external stimulation and self-perception of a human being.

We also imitated the hand and let our e-skin touch a cup of hot water (about 87 °C), as shown in Figure 5d. When the e-skin touches the hot water cup, it will have a positive voltage signal, and a negative voltage signal will be obtained when the e-skin moves away from the cup. It can be seen from the above experimental data that our e-skin is already very close to the function of human skin in sensing the body's mechanical movement and temperature change.

Pressure and Temperature Distribution Mapping. For applications in artificial e-skin, integrating multiple sensors to form a large-area flexible sensor array is desired for the detection of spatially resolved pressure and temperature. As a proof-of-concept, we fabricated an e-skin matrix of 16 pixels (4 × 4 elements). As shown in Figure 6a, different weights are placed on the different positions in the matrix, and the spatial distribution of external pressure could be easily detected by measuring their voltage changes. The voltage distribution is shown as the height of each pixel bar. This result is similar to

DOI: 10.1021/acsnano.8b04244
ACS Nano 2018, 12, 8588−8596

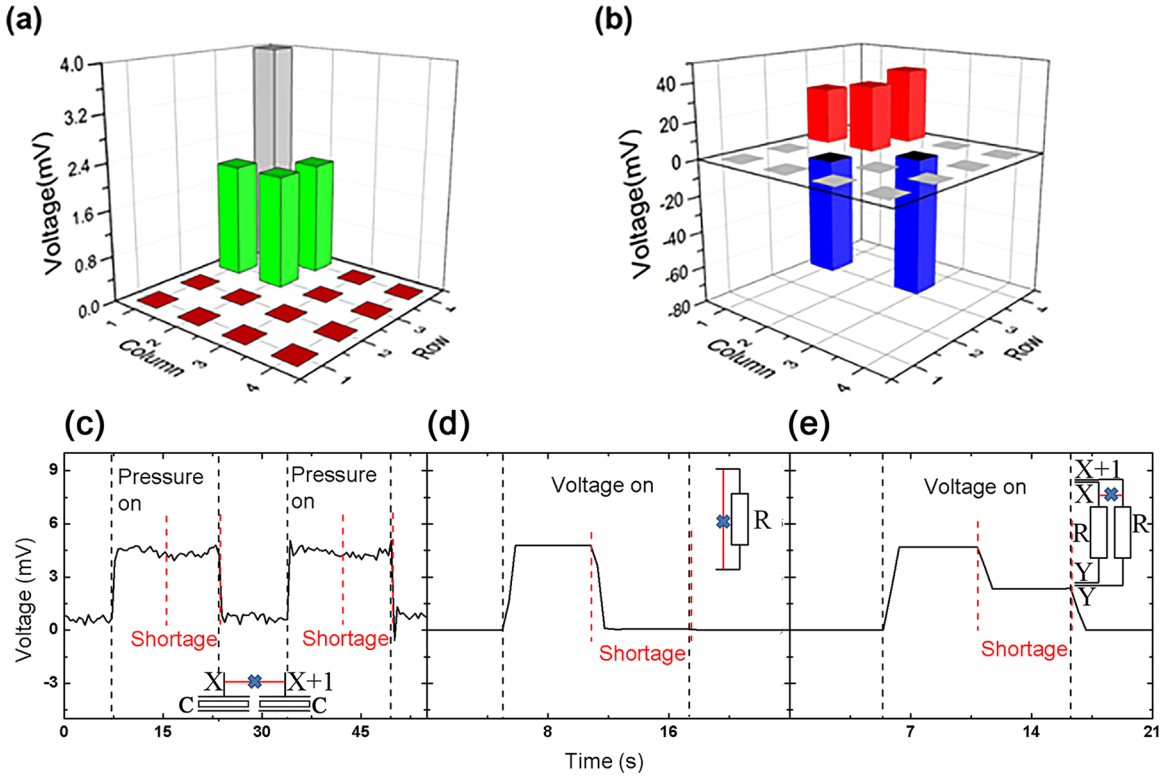

Figure 6. Detection of (a) different pressures and (b) heating or cooling, distributed on the pixelated sensor arrays. Unit output signal of a (c) single-electrode piezoelectric unit interrupted by a shortage between neighboring units, (d) resistance unit interrupted by a direct shortage, and (e) resistance unit interrupted by a shortage between neighboring units.

other studies.[14,34,35] The e-skin matrix can not only detect the pressure distribution but also detect the temperature distribution and distinguishes between heating and cooling. As shown in Figure 6b, the positive voltage means heating, the negative voltage means cooling, and the height of the pixel indicates the temperature difference; the bigger the difference between the temperature of the contact object, the larger the output voltage of the e-skin. Note that the size of the output signal is independent of the area of the membrane, as shown in Figure 4b, so the resolution of the e-skin array can be easily adjusted by changing the number and size of the electrodes, to achieve the different sensitivity requirements of the different parts of the intelligent robot.

Unlike traditional touch screens, electronic skin is used in a flexible environment and is therefore more susceptible to environmental damage, just as human skin often suffers from bruises or cuts. However, natural damage can easily lead to short-circuiting of the electrodes, which can lead to signal abnormalities. Therefore, we studied the signal changes under different short-circuit conditions. Figure 6c–e show the effect of short-circuiting on different units. In single-electrode piezoelectric electronic skin applications, there is no problem of short-circuiting the sensing unit itself, and there is only a short-circuit risk of signals between adjacent units. Figure 6c shows the signal condition of this device when a neighboring cell is short-circuited. It can be seen that the output signal is hardly affected by the short circuit. Traditional resistive devices are strongly affected. As can be seen in Figure 6d, when the resistive element itself is short-circuited, the output signal disappears. Although this signal can be screened out by the program, the effect of the short-circuiting of the neighboring cells is even more complicated. As shown in Figure 6e, the output signal is only reduced rather than disappearing, resulting in a false signal. It can be seen from this that single-electron piezoelectric electronic skin shows an excellent stability.

This work also shows that single-electrode components are not limited to TENGs. A self-powered component may achieve all this in principle. Since its working principal is the changing of electric potential, the chemical-sensing properties of this sensor can also be further studied.[36,37] The single-electrode configuration will have a lower risk of short-circuiting, increasing the reliability of the sensing unit, especially in applications with shape changes. Such an innovation will introduce flexible skin for a robot or human skin that can be connected to the nervous system. Better biocompatibility and practical mapping circuit design should be investigated in future research. Covering the surface with a soft antistatic material in these studies will greatly increase the useful life of the device.

CONCLUSIONS

We have fabricated a self-powered, transparent, and flexible e-skin based on SPENGs, which introduces another single-electrode electronic component besides previously reported TENGs. The single electrode of this sensor makes the pressure-sensing signal become a steady-state signal, while the pyroelectric signal appears as a pulse because of the leakage current effect. Benefiting from this, the sensor can work as an e-skin unit that can sense pressure and temperature at the same time. The pressure-sensing voltage is related only to the pressure strength and is independent of the sensor area, so that the sensor unit can continue to be microminiaturized. When ITO is used as a bottom electrode, the sensor can be changed

DOI: 10.1021/acsnano.8b04244
ACS Nano 2018, 12, 8588–8596

to a transparent sensor and thus applied to a transparent interface. The use of a portable electrospinning device allows the single electrode to be quickly functionalized for rapid application. Such an e-skin can also be fabricated in a scalable and cheap method.

EXPERIMENTAL SECTION

Materials. PVDF powder (M_w ~550 000, Shanghai 3F New Material Co., Ltd.) was used in this work. *N*,*N*-Dimethylformamide (DMF) was obtained from Sinopharm Chemical Reagents. Acetone was obtained from the Laiyang Fine Chemical Factory, China. Other materials include ITO conductive plastic film (Beijing JJAM Co., Ltd.) and aluminum foil.

Preparation of Solutions for Electrospinning. A PVDF solution was prepared by dissolving PVDF powder (22 wt %) in an acetone−DMF solvent mixture (1/1 w/w) and then stirring the mixture with a magnetic stir bar for 4 h at 50 °C.

Fabrication of the E-Skin. The fabrication process is designed to enable rapid device production, high yield, and high uniformity. Specifically, the process flow (Figure 1a) uses electrospinning to increase the speed, yield, and uniformity of the e-skin production. First, to simulate the robot surface, an insulating material (for example, glove and plastics) was chosen as a substrate. Then, the electrode array was fabricated on the substrate material by magnetron sputtering according to different resolution requirements. Finally, a functional layer was formed on the electrode layer by electrospinning to complete the e-skin. Here we used a homemade hand-held electrospinning device. The functional layer material is PVDF. Figure 1b shows the changes in the PVDF molecular structure during electrospinning. PVDF can change from α- to β-phase by electrospinning.[24] So it has excellent piezoelectric and pyroelectric properties. Figure 1c shows a photograph of the process of fabricating the e-skin by using a hand-held electrospinning device. Utilizing the homemade hand-held electrospinning device (a structure diagram of this device is shown in Figure S2b) enables easy and quick *in situ* preparation of the e-skin in some narrow places, solving the problem of bulky, large electrospinning equipment.

Characterizations. SEM (JSM-6700F) was used to characterize the morphology and dimensions of the ultrathin fibers. The digital multimeter (Rigol DM 3058) was used to record changes in the open-circuit voltage of the e-skin when it is subjected to external pressure or perceived temperature changes. In order to provide pressure on the e-skin, we used homemade pressure equipment that could exert periodic impact force. In order to provide different temperatures, a flexible commercial polyimide heater served to quickly change the temperature of the device. Current−voltage (I−V) curves were obtained by combining a Keithley 6487 and an Itech 6322 with a Quantum Design physical property measurement system via a P1 user bridge.

ASSOCIATED CONTENT

Supporting Information

The Supporting Information is available free of charge on the ACS Publications website at DOI: 10.1021/acsnano.8b04244.

Figures S1−S12: Concept and additional experimental details (PDF)

AUTHOR INFORMATION

Corresponding Author

*E-mail: yunze.long@163.com or yunze.long@qdu.edu.cn.

ORCID

Zhiyong Fan: 0000-0002-5397-0129
Seeram Ramakrishna: 0000-0001-8479-8686
Yun-Ze Long: 0000-0002-4278-4515

Author Contributions

⊥X.-X. Wang and W.-Z. Song contributed equally.

Notes

The authors declare no competing financial interest.

ACKNOWLEDGMENTS

This work was supported by the National Natural Science Foundation of China (51673103), the Shandong Provincial Natural Science Foundation, China (ZR2017BA013), the China Postdoctoral Science Foundation (2017M612200), and the Postdoctoral Scientific Research Foundation of Qingdao (2016007 and 2016014).

REFERENCES

(1) Goldberg, K. Robotics: Countering Singularity Sensationalism. *Nature* **2015**, *526*, 320−321.

(2) Everingham, M.; Eslami, S. M. A.; Van Gool, L.; Williams, C. K. I.; Winn, J.; Zisserman, A. The PASCAL Visual Object Classes Challenge: A Retrospective. *Int. J. Comput. Vision* **2015**, *111*, 98−136.

(3) Hou, C. Y.; Wang, H. Z.; Zhang, Q. H.; Li, Y. G.; Zhu, M. F. Highly Conductive, Flexible, and Compressible All-Graphene Passive Electronic Skin for Sensing Human Touch. *Adv. Mater.* **2014**, *26*, 5018−5024.

(4) Vural, M.; Behrens, A. M.; Ayyub, O. B.; Ayoub, J. J.; Kofinas, P. Sprayable Elastic Conductors Based on Block Copolymer Silver Nanoparticle Composites. *ACS Nano* **2015**, *9*, 336−344.

(5) Li, X.; Lin, Z.-H.; Cheng, G.; Wen, X.; Liu, Y.; Niu, S.; Wang, Z. L. 3D Fiber-Based Hybrid Nanogenerator for Energy Harvesting and as a Self-Powered Pressure Sensor. *ACS Nano* **2014**, *8*, 10674−10681.

(6) Wang, C. H.; Lai, K. Y.; Li, Y. C.; Chen, Y. C.; Liu, C. P. Ultrasensitive Thin-Film-Based $Al_xGa_{1-x}N$ Piezotronic Strain Sensors *via* Alloying-Enhanced Piezoelectric Potential. *Adv. Mater.* **2015**, *27*, 6289−6295.

(7) Park, D. Y.; Joe, D. J.; Kim, D. H.; Park, H.; Han, J. H.; Jeong, C. K.; Park, H.; Park, J. G.; Joung, B.; Lee, K. J. Self-Powered Real-Time Arterial Pulse Monitoring Using Ultrathin Epidermal Piezoelectric Sensors. *Adv. Mater.* **2017**, *29*, 1702308.

(8) Lipomi, D. J.; Vosgueritchian, M.; Tee, B. C. K.; Hellstrom, S. L.; Lee, J. A.; Fox, C. H.; Bao, Z. N. Skin-Like Pressure and Strain Sensors Based on Transparent Elastic Films of Carbon Nanotubes. *Nat. Nanotechnol.* **2011**, *6*, 788−792.

(9) Someya, T.; Sekitani, T.; Iba, S.; Kato, Y.; Kawaguchi, H.; Sakurai, T. A Large-Area, Flexible Pressure Sensor Matrix with Organic Field-Effect Transistors for Artificial Skin Applications. *Proc. Natl. Acad. Sci. U. S. A.* **2004**, *101*, 9966−9970.

(10) Someya, T.; Kato, Y.; Sekitani, T.; Iba, S.; Noguchi, Y.; Murase, Y.; Kawaguchi, H.; Sakurai, T. Conformable, Flexible, Large-Area Networks of Pressure and Thermal Sensors With Organic Transistor Active Matrixes. *Proc. Natl. Acad. Sci. U. S. A.* **2005**, *102*, 12321−12325.

(11) Chen, J.; Zhu, G.; Yang, W. Q.; Jing, Q. S.; Bai, P.; Yang, Y.; Hou, T. C.; Wang, Z. L. Harmonic-Resonator-Based Triboelectric Nanogenerator as a Sustainable Power Source and a Self-Powered Active Vibration Sensor. *Adv. Mater.* **2013**, *25*, 6094−6099.

(12) Wang, S. H.; Mu, X. J.; Yang, Y.; Sun, C. L.; Gu, A. Y.; Wang, Z. L. Flow-Driven Triboelectric Generator for Directly Powering a Wireless Sensor Node. *Adv. Mater.* **2015**, *27*, 240−248.

(13) Wang, X. D.; Zhang, H. L.; Dong, L.; Han, X.; Du, W. M.; Zhai, J. Y.; Pan, C. F.; Wang, Z. L. Self-Powered High-Resolution and Pressure-Sensitive Triboelectric Sensor Matrix for Real-Time Tactile Mapping. *Adv. Mater.* **2016**, *28*, 2896−2903.

(14) Chen, J. K.; Ding, P.; Pan, R. Z.; Xuan, W. P.; Guo, D. P.; Ye, Z.; Yin, W. L.; Jin, H.; Wang, X. Z.; Dong, S. R.; Luo, J. K. Self-Powered Transparent Glass-Based Single Electrode Triboelectric Motion Tracking Sensor Array. *Nano Energy* **2017**, *34*, 442−448.

(15) Guo, H. J.; Li, T.; Cao, X. T.; Xiong, J.; Jie, Y.; Willander, M.; Cao, X.; Wang, N.; Wang, Z. L. Self-Sterilized Flexible Single-

DOI: 10.1021/acsnano.8b04244
ACS Nano 2018, 12, 8588−8596

Electrode Triboelectric Nanogenerator for Energy Harvesting and Dynamic Force Sensing. *ACS Nano* **2017**, *11*, 856−864.
(16) Tao, M. M.; Xue, L. X.; Liu, F.; Jiang, L. An Intelligent Superwetting PVDF Membrane Showing Switchable Transport Performance for Oil/Water Separation. *Adv. Mater.* **2014**, *26*, 2943−2948.
(17) Zhang, W. B.; Shi, Z.; Zhang, F.; Liu, X.; Jin, J.; Jiang, L. Superhydrophobic and Superoleophilic PVDF Membranes for Effective Separation of Water-in-Oil Emulsions with High Flux. *Adv. Mater.* **2013**, *25*, 2071−2076.
(18) Persano, L.; Dagdeviren, C.; Su, Y. W.; Zhang, Y. H.; Girardo, S.; Pisignano, D.; Huang, Y. G.; Rogers, J. A. High Performance Piezoelectric Devices Based on Aligned Arrays of Nanofibers of Poly(vinylidenefluoride-co-trifluoroethylene). *Nat. Commun.* **2013**, *4*, 1633.
(19) Shin, K. Y.; Lee, J. S.; Jang, J. Highly Sensitive, Wearable and Wireless Pressure Sensor Using Free-Standing ZnO Nanoneedle/PVDF Hybrid Thin Film for Heart Rate Monitoring. *Nano Energy* **2016**, *22*, 95−104.
(20) You, M. H.; Wang, X. X.; Yan, X.; Zhang, J.; Song, W. Z.; Yu, M.; Fan, Z. Y.; Ramakrishna, S.; Long, Y. Z. A Self-Powered Flexible Hybrid Piezoelectric-Pyroelectric Nanogenerator Based on Non-Woven Nanofiber Membranes. *J. Mater. Chem. A* **2018**, *6*, 3500−3509.
(21) Zheng, J. F.; He, A. H.; Li, J. X.; Han, C. C. Polymorphism Control of Poly(vinylidene fluoride) Through Electrospinning. *Macromol. Rapid Commun.* **2007**, *28*, 2159−2162.
(22) Yee, W. A.; Kotaki, M.; Liu, Y.; Lu, X. H. Morphology, Polymorphism Behavior and Molecular Orientation of Electrospun Poly(Vinylidene Fluoride) Fibers. *Polymer* **2007**, *48*, 512−521.
(23) Mandal, D.; Yoon, S.; Kim, K. J. Origin of Piezoelectricity in an Electrospun Poly(vinylidene fluoride-trifluoroethylene) Nanofiber Web-Based Nanogenerator and Nano-Pressure Sensor. *Macromol. Rapid Commun.* **2011**, *32*, 831−837.
(24) Zheng, J.; He, A.; Li, J.; Han, C. C. Polymorphism Control of Poly(vinylidene fluoride) through Electrospinning. *Macromol. Rapid Commun.* **2007**, *28*, 2159−2162.
(25) Tawansi, A.; Oraby, A. H.; Badr, S. I.; Elashmawi, I. S. Physical Properties and B-Phase Increment of $AgNO_3$-Filled Poly(vinylidene fluoride) Films. *Polym. Int.* **2004**, *53*, 370−377.
(26) Chu, T. L.; Weissman, S. I. Symmetry Classification of the Energy Levels of Some Triarylmethyl Free Radicals and Their Cations. *J. Chem. Phys.* **1954**, *22*, 21−25.
(27) Yang, Y.; Zhou, Y. S.; Zhang, H.; Liu, Y.; Lee, S.; Wang, Z. L. A Single-Electrode Based Triboelectric Nanogenerator as Self-Powered Tracking System. *Adv. Mater.* **2013**, *25*, 6594−6601.
(28) Lee, J. H.; Lee, K. Y.; Gupta, M. K.; Kim, T. Y.; Lee, D. Y.; Oh, J.; Ryu, C.; Yoo, W. J.; Kang, C. Y.; Yoon, S. J. Highly Stretchable Piezoelectric-Pyroelectric Hybrid Nanogenerator. *Adv. Mater.* **2014**, *26*, 765−769.
(29) Bowen, C.; Wan, C. Multiscale-Structuring of Polyvinylidene Fluoride for Energy Harvesting: the Impact of Molecular-, Micro- and Macro-Structure. *J. Mater. Chem. A* **2017**, *5*, 3091−3128.
(30) Tien, N. T.; Seol, Y. G.; Dao, L. H. A.; Noh, H. Y.; Lee, N. E. Utilizing Highly Crystalline Pyroelectric Material as Functional Gate Dielectric in Organic Thin-Film Transistors. *Adv. Mater.* **2010**, *21*, 910−915.
(31) Yang, Y.; Zhang, H.; Zhu, G.; Lee, S.; Lin, Z. H.; Wang, Z. L. Flexible Hybrid Energy Cell for Simultaneously Harvesting Thermal, Mechanical, and Solar Energies. *ACS Nano* **2013**, *7*, 785−90.
(32) Niu, S.; Liu, Y.; Wang, S.; Lin, L.; Zhou, Y. S.; Hu, Y.; Wang, Z. L. Theoretical Investigation and Structural Optimization of Single-Electrode Triboelectric Nanogenerators. *Adv. Funct. Mater.* **2014**, *24*, 3332−3340.
(33) Leng, Q.; Chen, L.; Guo, H.; Liu, J.; Liu, G.; Hu, C.; Xi, Y. Harvesting Heat Energy from Hot/cold Water with a Pyroelectric Generator. *J. Mater. Chem. A* **2014**, *2*, 11940−11947.
(34) Hu, W.; Zhang, B.; Luo, W.; Zhang, J.; Guo, Y.; Chen, S.; Yun, M.; Ramakrishna, S.; Long, Y. Z. Ag/alginate Nanofiber Membrane for Flexible Electronic Skin. *Nanotechnology* **2017**, *28*, 445502.
(35) Wang, C.; Xia, K.; Zhang, M.; Jian, M.; Zhang, Y. An All Silk-Derived Dual-Mode E-skin for Simultaneous Temperature-Pressure Detection. *ACS Appl. Mater. Interfaces* **2017**, *9*, 39484−39492.
(36) Yang, D. P.; Guo, W. W.; Cai, Z. F.; Chen, Y. S.; He, X. S.; Huang, C. S.; Zhuang, J. Y.; Jia, N. Q. Highly Sensitive Electrochemiluminescence Biosensor for Cholesterol Detection Based on Agnps-BSA-MnO_2 Nanosheets with Superior Biocompatibility and Synergistic Catalytic Activity. *Sens. Actuators, B* **2018**, *260*, 642−649.
(37) Zhong, S. L.; Zhuang, J. Y.; Yang, D. P.; Tang, D. P. Eggshell Membrane-Templated Synthesis of 3D Hierarchical Porous Au Networks for Electrochemical Nonenzymatic Glucose Sensor. *Biosens. Bioelectron.* **2017**, *96*, 26−32.

DOI: 10.1021/acsnano.8b04244
ACS Nano 2018, 12, 8588−8596